



**A retrospective study of the pre-eruptive unrest on El Hierro (Canary Islands):  
implications of seismicity and deformation in the short-term volcanic hazard  
assessment**

Stefania Bartolini<sup>1,a</sup>, Carmen López<sup>2</sup>, Laura Becerril<sup>1</sup>, Rosa Sobradelo<sup>3</sup>, Joan Martí<sup>1</sup>

<sup>1</sup> Group of Volcanology, (SIMGEO-UB) CSIC, Institute of Earth Sciences Jaume Almera, c/Lluis Sole Sabaris s/n, 08028 Barcelona, Spain.

<sup>2</sup> Observatorio Geofísico Central, Instituto Geográfico Nacional (IGN), c/Alfonso XII, 3, 28014 Madrid, Spain.

<sup>3</sup> Willis Research Network and Analytics Technology, Willis Towers Watson, London, UK.

<sup>a</sup> Corresponding author: Stefania Bartolini, Group of Volcanology, (SIMGEO-UB) CSIC, Institute of Earth Sciences Jaume Almera, c/Lluis Sole Sabaris s/n, 08028 Barcelona, Spain. ([sbartolini.1984@gmail.com](mailto:sbartolini.1984@gmail.com))

**Key points**

- Short-term spatio-temporal analysis for understanding unrest indicators during an unrest phase.
- A new methodology to be applied in short-term hazard assessment.
- Spatio-temporal analysis using information obtained from monitoring data.



1    **Abstract**

2    The correct identification and interpretation of unrest indicators are useful for  
3    forecasting volcanic eruptions, delivering early warnings, and understanding the  
4    changes occurring in a volcanic system prior to an eruption. Such indicators play an  
5    important role in upgrading previous long-term volcanic hazard assessments and help  
6    grasp the complexities of the preceding period of eruptive activity. In this work, we  
7    present a retrospective analysis of the 2011 unrest episode on the island of El Hierro  
8    that preceded a submarine eruption. We use seismic and surface deformation  
9    monitoring data to compute the susceptibility analysis (QVAST tool) and to study the  
10   evolution over time of the unrest (ST-HASSET tool). Additionally, we show the  
11   advantages to be gained by using continuous monitoring data and hazard assessment e-  
12   tools to upgrade spatio-temporal analyses and thus visualize more simply the  
13   development of the volcanic activity.

14

15    **Keywords**

16    Short-term volcanic hazard assessment, unrest, precursors, monitoring, spatio-temporal  
17    analysis

18

19

20

21

22

23

24

25



26 **1. Introduction**

27 The most challenging aspect of forecasting volcanic eruptions is the correct  
28 identification and interpretation of precursors during the episodes of unrest that  
29 normally precede eruptive activity. During this phase, the short-term volcanic hazard  
30 assessment can be computed by combining a long-term hazard analysis with real-time  
31 monitoring data, updating continuously the status of the volcanic hazard (Blong, 2000;  
32 Sobradelo and Martí, 2015; Tonini et al., 2016). Short-term evaluations can help  
33 forecast the likely outcomes – i.e. where and when the eruption will take place – by  
34 drawing on the information derived from indicators and an understanding of the  
35 volcanic system. The parameters associated with the volcanic process are the  
36 geophysical and geochemical signals that provide information on magma movement  
37 within the volcanic system and on how the magma is preparing to reach the surface  
38 (Chouet, 1996; McNutt, 1996).

39 In particular, the signals recorded during unrest episodes – for example, an  
40 increase in activity compared to the previous background level (Phillipson et al., 2013)  
41 – can be used to deduce changes in magma accumulation and movement, the state of  
42 stress of the host rock, and the physical and chemical properties of the magma itself  
43 (Harrington and Brodsky, 2007; Jellinek and Bercovici, 2011; Lavallée et al., 2008;  
44 McNutt, 2005; Neuberg et al., 2000; Papale, 1999; Tárraga et al., 2014). A  
45 comprehensive well organized monitoring network on and around the volcano is  
46 fundamental if scientists are to analyze how the eruption process is evolving. Changes  
47 may be detected on the surface that reflect variations in the geophysical (e.g. seismicity,  
48 surface deformation, and changes in potential fields) and/or geochemical (e.g. gas flow  
49 rate and gas composition) parameters sensed by the network that is monitoring the



50 activity of the volcano (Scarpa and Tilling, 1996; Sparks, 2003; Vallianatos et al., 2013,  
51 Telesca et al., 2015).

52 It is essential that all the monitoring information obtained during an unrest phase  
53 be processed and interpreted in real time. This is a crucial consideration since this  
54 information is vital in eruption forecasting and provides support for decision-makers. In  
55 many instances during an unrest phase, the institution in charge of the monitoring  
56 network is expected to publish daily or even hourly bulletins with updates derived from  
57 monitoring signals. These bulletins are then used by experts (e.g. a scientific committee  
58 or crisis team) to keep public officials abreast of the state of the volcanic system. These  
59 reports do not generally contain probabilistic model results and tend to consist merely  
60 of processed monitoring data related to seismicity, deformation, and gas emissions.

61 In order to provide a simple and automated way of assessing the evolution of the  
62 volcanic system from looking at the monitoring signals, the ST-HASSET was  
63 developed (Sobradelo and Martí, 2015; Bartolini et al., 2016). This e-tool offers an  
64 alternative to the BET-EF (Marzocchi et al., 2008) and BET-UNREST (Tonini et al.,  
65 2016) and also proposes a flexible probabilistic approach to incorporate monitoring  
66 information for the quantification of short-term volcanic hazard that looks for  
67 significant changes in the values of the measured unrest indicators, across consecutive  
68 time intervals. In comparison to the BET-EF and BET-UNREST, ST-HASSET does not  
69 focus on the absolute value of each variable with respect to a defined threshold, but  
70 compares its degree of change with respect to the previous time interval. In each case, a  
71 variation that is considered significant can be defined in advance given the specific  
72 characteristics of the volcano being studied.

73 Assuming that the geophysical indicators such as seismicity and ground  
74 deformation provide insights on the location of magma during the unrest phase (Endo



75 and Murray, 1991; Chouet, 1996; McNutt, 1996; Martí et al., 2013), changes in the  
76 location of such unrest parameters may indicate magma movement and, consequently,  
77 that the location of potential new vents may also change. This is extremely important  
78 when conducting hazard assessment analysis, as the location of the eruptive vent may  
79 condition the resulting hazards and their potential impacts. In this sense, short-term  
80 hazard assessment needs to inform in real time on how monitoring information changes  
81 the probabilities of vent opening (volcanic susceptibility) and of the hazards that may  
82 occur, as well as of the proximity of the eruptive event.

83 In order to show how ST-HASSET works, we apply it retrospectively to the  
84 unrest episode that preceded the El Hierro eruption in 2011. When volcanic unrest  
85 started here in July 2011, the Spanish National Geographical Institute (IGN), the  
86 institution responsible for volcano monitoring in Spain, set up a dense seismic  
87 monitoring network composed of a three-component (3CC) broadband station (CTIG)  
88 and eight short- and medium-period (natural periods of 1 and 5 s) 3CC stations (López  
89 et al., 2012) (Fig. 1). In order to monitor the associated 3D deformation, the IGN also  
90 deployed four extra GPS stations on El Hierro to reinforce the capacity of the single  
91 pre-existing GPS station (FRON) (Fig. 1) belonging to the Canary Regional  
92 government (López et al., 2012, 2014; Martí et al., 2013). The amount of information  
93 registered provides a good example of a monitored unrest episode with a complete  
94 dataset. However, during the pre-eruptive unrest phase the continuous changes in the  
95 position of the seismicity and deformation sources made it all but impossible to forecast  
96 the position of the new vent and, consequently, to define reliable eruption scenarios.

97 The objective of this retrospective analysis is to define guidelines on how we  
98 can manage the information generated by a monitoring network during the unrest phase  
99 of an ongoing crisis. We use the data recorded in the pre-eruptive unrest episode that



100 took place on El Hierro in 2011 to update in real time the spatial probability of the new  
101 vent opening and to interpret the unrest precursors as a means of determining the  
102 probability of evolution of these indicators. So, we first evaluate the volcanic  
103 susceptibility combining the real time monitoring information with the QVAST tool  
104 (Bartolini et al., 2013), which provides a real time variation of the vent opening  
105 probabilities. Then, we combine each updated result with the ST-HASSET tool to  
106 determine the evolution over time of the unrest indicators. The results obtained allow us  
107 to realise how the application of these tools helps interpret the unrest indicators and how  
108 they can be used for improving the susceptibility assessment and the definition of  
109 realistic eruptive scenarios, thus facilitating the decision making process and the  
110 management of the volcanic crisis.

111

## 112 **2. Methodology**

113 The methodology used in this study basically consists in the systematic  
114 application of two e-tools specifically designed for conducting probabilistic spatial and  
115 temporal analysis in volcanic hazard assessment.

116 QVAST (Bartolini et al., 2013) is a tool that has been developed to evaluate the  
117 spatial probability of a new vent opening (volcanic susceptibility) using volcano-  
118 structural data and seismicity. In monogenetic volcanism, as it is the case of El Hierro,  
119 each new eruption creates a different vent, which indicates that accurate spatial  
120 forecasting is highly uncertain. This type of analysis has been often applied in long-term  
121 hazard assessment as it represents a good starting point for developing hazard maps  
122 based on certain assumptions: i) future eruptive vents will be close to the previous ones  
123 and ii) the stress field plays the most significant role in determining where magma will  
124 reach the surface (see Martí et al., 2016). The result is a (long-term) susceptibility map



125 obtained by assigning different weights to each of the probability density functions in  
126 each dataset (volcano-structural elements: location of past vents, eruptive fissures,  
127 fractures, faults, dykes, etc.) considered in the analysis, which are combined via a  
128 weighted sum and modelled in a non-homogeneous Poisson process. During an unrest  
129 phase, the (short-term) susceptibility map varies as new information (e.g. the location of  
130 the seismic events) is provided by monitoring data. Hence, the previously defined  
131 probabilities of hosting a new vent will change in terms of where the new seismicity  
132 and/or ground deformation is located — assuming that both parameters provide an  
133 indication of magma movement and location.

134 The probability of occurrence of a possible eruptive scenario will change  
135 according to the variations in the short-term susceptibility map, which will be redefined  
136 each time that new monitoring information will be computed; thus, we also have to  
137 calculate the temporal evolution of monitoring data.

138 The ST-HASSET tool (Sobradelo and Martí, 2015; Bartolini et al., 2016) is a  
139 simple tool that develops an event tree structure that uses a quantitative approach via  
140 Bayesian inference to assess the hazard of a particular volcanic scenario by taking into  
141 account monitoring data and all relevant data pertaining to the past history of the  
142 volcano. Indicators are shown on a common probability scale to visualize their progress  
143 during the unrest phase and to estimate the probability of occurrence of a particular  
144 eruptive scenario.

145

### 146 **3. Unrest on El Hierro in 2011**

147 El Hierro, situated in the southwestern corner of the Canary archipelago (Fig. 1), is  
148 geologically the youngest of these islands and its oldest subaerial rocks have been dated  
149 at 1.12 Ma (Guillou et al., 1996). It corresponds to a shield structure formed by different



150 volcanic edifices with three rift zones along which recent volcanism has been  
151 concentrated (Guillou et al., 1996). The studied unrest period started on 19 July 2011  
152 and gave rise to a submarine eruption that started on 10 October 2011 (Fig. 1). The  
153 whole episode was well monitored by the IGN and during the period leading up to the  
154 eruption approximately 10,000 earthquakes with local magnitudes of up to 4.3 were  
155 recorded, and over 5 cm of vertical and horizontal surface deformations were registered  
156 (López et al., 2014).

157         This pre-eruptive unrest started with a marked increase in seismicity, followed a  
158 few days later by surface deformation and gas emissions (López et al., 2012). The  
159 evolution of the seismicity during this episode was characterized by changes in the  
160 hypocentral location that were interpreted as movements in the position of the magma  
161 (Fig. 2 and Table 1) (López et al., 2012, 2014). During the first weeks of unrest, all the  
162 seismic events were located in the north of the island at a depth of about 10–15 km b.s.l.  
163 and were of low magnitude. As of 4–26 September 2011, the seismicity migrated  
164 southwards along the crust/mantle boundary and the amount of released seismic energy  
165 increased. GPS stations began also to rotate to the North, suggesting a simultaneous  
166 surface deformation pattern that reflected a correlated migration of the pressure source  
167 towards the south. From 27 September to 7 October 2011, both the seismic rate and the  
168 seismic energy grew and events were now located mostly off the SW coast of El Hierro.  
169 At the same time, a sudden deflation–re-inflation was observed on the N–S component at  
170 all GPS stations (1–5 October 2011). On 8 October at 20:34 h (GMT), a 4.3 ML  
171 earthquake (the greatest magnitude recorded during the unrest period) occurred 1.5 km  
172 off the SW coast of the island at a depth of 12 km. However, from this moment  
173 onwards, very few further earthquakes were registered and the pre-eruptive episode  
174 culminated with a submarine eruption on the southern flank of the island’s volcanic



175 edifice (López et al., 2012) (Fig. 1). On 10 October at 04:10 UTC, a clear emergent  
176 tremor signal was registered by all the seismic stations indicating the onset of the  
177 eruptive activity that lasted for more than four months (until the end of February 2012)  
178 (López et al., 2014).

179

#### 180 **4. Datasets**

##### 181 4.1 Spatial analysis

182 A susceptibility analysis enables us to determine the probability of occurrence of future  
183 eruptive vents. This probability depends on the volcano-structural elements that define  
184 the structural setting of a volcano and the past pathways taken by the magma as it  
185 ascended to the Earth's surface. Eruptive vents and fissures, dykes, faults, fumaroles,  
186 and the stress field are the most important elements (Martin et al., 2004; Jaquet et al.,  
187 2008; Cappello et al., 2012; Bartolini et al., 2013; and references therein) that determine  
188 the probabilities of an eruptive vent opening in an area that was affected by similar  
189 types of eruptions in the past.

190 In order to compute the probability of opening a new eruptive vent at El Hierro,  
191 we took into account the most relevant volcano-structural data as given by Becerril et al.  
192 (2013, 2014) (Fig. 2): (i) the subaerial vents and eruptive fissures that are part of the  
193 Rift Volcanism (including sub-recent and recent eruptions) and (ii) the submarine vents  
194 and eruptive fissures deduced from bathymetric inference. Furthermore, we chose only  
195 those eruptive fissures oriented between N00°E and N45°E in relation to the orientation  
196 of the regional stress field (see Geyer et al., 2016). We assumed that the stress field  
197 plays the most important role in determining where the magma will reach the surface  
198 and the fractures orientated in this direction were those that offered the least resistance  
199 to magma transport.



200 To conduct the short-term analysis, we complemented the previous dataset with  
201 the addition of data on the evolution of the seismicity for the unrest period (19 July  
202 2011–10 October 2011).

203 We assumed that in this short-term spatial analysis the location of the seismicity  
204 reflected the position of the magma, as it provides a good indicator for tracking magma  
205 migration and for determining where it may potentially reach the surface. However, the  
206 location of gas emission was not considered in this short term analysis as they were too  
207 disperse in the whole area (López et al., 2012) and thus not sufficiently informative on  
208 the position that magma could have below the island. Concerning the surface  
209 deformation, we considered this parameter only in the temporal analysis, due to the lack  
210 of a well-distributed ground deformation monitoring network operating during the El  
211 Hierro unrest episode. So, as described in López et al. (2012), the highest values of  
212 uplift were found in the area where the seismicity moved from north to south and where  
213 no GPS was available.

214 Seismic data was obtained from the seismic catalogue published by the Spanish  
215 National Geographical Institute (IGN) ([www.ign.es](http://www.ign.es)) (Fig. 2). Data was grouped in time  
216 windows of four days to optimize the forecast given that certain volcanic systems have  
217 indicated that magmatic processes have a memory with a time-scale of just a few days.  
218 (Connor et al., 2003; Jaquet and Carniel, 2003; Jaquet et al., 2006; Tárraga et al., 2006;  
219 Carniel et al., 2006). Such a selection allows assuring the persistent behaviors of the  
220 system. Within the time window, the seismic activity will follow the same trend of  
221 previous days, allowing the short-term forecast. We selected from the IGN catalogue  
222 only those earthquakes of magnitudes greater than zero and precise locations, with  
223 epicenter maximum semi-ellipse axes of less than 15 km, minimum semi-ellipse axes of  
224 less than 6 km, and a depth error of less than 8 km. In this way, we aimed to avoid –



225 inasmuch as was possible – errors in the hypocenter localization of earthquakes due to  
226 the small number of the seismic stations in place during the first unrest phase.

227

#### 228 4.2 Temporal analysis

229 The data for the temporal analysis consisted of observables which relative variation  
230 with time may indicate changes in the processes occurring inside the volcano when  
231 preparing for a new eruption (Sobradelo and Martí, 2015; Bartolini et al., 2016). In our  
232 methodology, we do not use the absolute values of each parameter, but considering their  
233 relative variation with time, we only indicate if there is an increase or a decrease in the  
234 value of such parameter in each time interval. We used the monitoring data gathered by  
235 the IGN and other published information (López et al., 2012, 2014; Martí et al., 2013;  
236 Telesca et al., 2014). This information is given in Table 1 and includes:

- 237 - the number of seismic events
- 238 - RSAM (Real-time Seismic Amplitude Measurement)
- 239 - the seismic energy released during the fracturing process
- 240 - the lateral and vertical migration of the seismicity
- 241 - the number of shallow seismic events
- 242 - the strain variation.

243 Therefore, consistent with the choices adopted for the spatial analysis, the  
244 variation in the unrest indicators (increase/decrease) was evaluated in relation to the  
245 mean values for the previous four days. The seismic rate variation was considered by  
246 taking into account only those events with a magnitude over 2.5 (greater than the  
247 completeness magnitude during almost all the period), assuring this way the study of the  
248 seismic evolution (López et al., 2017), while a significant change was considered only  
249 when the rate of variation was 25% higher in relation to the previous four days as a



250 consequence of stress reorganization (Stein, 1999). RSAM data was obtained by  
251 analyzing the signal registered by the vertical component of the seismic broadband  
252 CTIG station (Fig. 1). Although the signal may have a high background of seismic  
253 noise, a RSAM increase is a good indicator of the transport of the magma to the surface  
254 (Endo and Murray, 1991). In order to highlight a significant increase in RSAM values,  
255 we considered the variation in the slope of the inverse of the RSAM, which is clear  
256 evidence of a consistent increase in the signal. The accumulated increase in energy  
257 release was considered to be significant when the energy value (i.e. the accumulated  
258 value in relation to the mean value over the last four days) was greater than 10%. In this  
259 case, the accumulated energy curve showed a notable slope variation. For the lateral  
260 migration of the seismicity, we considered a significant variation to exist when the  
261 displacement increment was over 1 km. This is compatible with the effects on hazard  
262 scenarios when the vent location changes. The vertical migration of the seismicity  
263 ranges from a depth of approximately 19 km to the surface and, taking into account the  
264 mean of the variation, a variation greater than 0.6 km was assumed to be notable. The  
265 number of shallow events reflects the presence of the magma close to the surface and so  
266 we assumed that the number of events of magnitude greater than 3 in the same day at a  
267 depth of 0–5 km was significant. Finally, the strain variation has been determined with  
268 the horizontal components data of the GPS FRON station. We have assumed a  
269 significant variation when the increase/decrease was greater than 1.5 mm of the vector  
270 representing the horizontal deformation (composing the north and east GPS  
271 components).

272

273

274 **5. Results**



## 275 **5.1 Spatial probability of new vent opening**

276 Given its great flexibility and ability to identify the most likely zones to host new  
277 eruptions in monogenetic volcanic fields, we used the QVAST tool (Bartolini et al.,  
278 2013) to determine the susceptibility from the evolution of the seismicity during the  
279 unrest. This tool was applied first to evaluate the smoothing factors (bandwidths) of the  
280 dataset analysed, then to evaluate the probability density functions for each dataset, and,  
281 finally, to calculate the final susceptibility map (Fig. 3) (see also Figure S1).

282 In the case of the rift volcanism and the submarine layers, we applied the Least  
283 Square Cross Validation Method (LSCV) (Cappello et al., 2012; Bartolini et al., 2013)  
284 to obtain the bandwidth parameter (see Becerril et al. (2013)). To determine the  
285 influence of seismicity in the spatial analysis, we considered that the most  
286 representative result was that obtained using Silverman's Rule of Thumb for the optimal  
287 bandwidth (Silverman, 1986). Thus, we obtained a bandwidth value of 1100 m for the  
288 rift volcanism and of 3900 m for the submarine layer, while in the case of the seismic  
289 data the range in the degree of randomness was from 500 m to 1500 m.

290 In the evaluation of the final susceptibility, weights were assigned based on  
291 expert opinion and on previously published work (Becerril et al., 2013, 2014), and by  
292 taking into account the average depth of the seismicity during the unrest episode.  
293 Specifically, up to 7 October we observed no significant variation in the shallow  
294 seismicity (Table 1). In this case, we assigned the following weights: 0.5 for seismic  
295 events, 0.3 for onshore vents and fissures, and 0.2 for offshore vents and fissures. In the  
296 final period (8–10 October), we considered the shallow earthquakes as a separate layer  
297 by assigning a different and more consistent weight as follows: 0.6 for shallow seismic  
298 events, 0.2 for the remaining seismic events, 0.1 for onshore vents and fissures, and 0.1  
299 for offshore vents and fissures.



300           The results shown in Figure 3 (see also Figure S1) highlight the importance of  
301 combining monitoring data with a previous long-term hazard assessment as a means of  
302 updating the probability of a new eruptive vent appearing in a particular area. The  
303 presence of previous volcanic structures does not provide sufficient information for  
304 forecasting the possible opening of a fresh vent during the unrest phase; however, if this  
305 information is combined with ongoing seismicity the predicted result can be improved.  
306 As shown in Figure 3, before the eruption the area with the highest probability of a  
307 fresh vent opening is the area that is closest to the eruptive vent.

308

## 309 **5.2 Evolution of unrest indicators and short-term hazard assessment**

310 The temporal analysis of the unrest indicators was conducted by applying the ST-  
311 HASSET tool (Bartolini et al., 2016) to analyze possible patterns in the evolution of  
312 events preceding the submarine eruption on El Hierro. The advantages of this tool lie in  
313 its ability to consider different signals on the same probabilistic scale, based on any  
314 significant or abnormal change in the unrest signal, with respect to a previous stage  
315 and/or a base-line measurement considered normal. The tool computes at each stage the  
316 probability of experiencing an anomalous change (increase/decrease) by the next time  
317 bulletin, based on what has been observed up until now. With this, it helps the scientist  
318 sum up the evolution of the unrest indicators and gets some insight into the possible  
319 unfolding of the volcanic crisis in the immediate future, helping with decision-making  
320 and the interpretation of the unrest. In Table 1, we show the data for the entire unrest  
321 period and, as explained in section 3.2.2, we considered the variation (“Y”) of the  
322 indicator analysed based on different criteria. The choice of the aleatoric and epistemic  
323 uncertainties (prior and data weights) surrounding the probability estimates were  
324 assumed considering that El Hierro unrest was the first unrest registered in Canaries.



325 The prior weights were assumed to be the probability results of the previous bulletin  
326 (only in the first simulation we have assumed the same probability for each indicator).  
327 In the case of the data weights, we have first assigned a total epistemic uncertainty and  
328 sequentially incremented the weight with the evolution of the unrest.

329 In Figure 4 and Movie S1, the evolution of the indicators over the entire unrest  
330 period with a daily time window are clearly visible. In the right side of the chart, it is  
331 shown also day-by-day the total number of parameters that increase or decrease during  
332 the unrest evolution. We assumed a value of +1 if the indicator increases, -1 if the  
333 indicator decreases, and 0 if the change is not significant. This allows visualizing the  
334 overall tendency of variation of the unrest indicators. We also considered three phases  
335 of 28 days, all three during the evolution of the unrest period, as shown in Figure 5 and  
336 so were able to observe how these indicators varied in different ways as the unrest  
337 evolved:

- 338 – Phase I: from July 19<sup>th</sup> to August 15<sup>th</sup>;
- 339 – Phase II: from the August 16<sup>th</sup> to September 12<sup>th</sup>;
- 340 – Phase III: from September 13<sup>th</sup> to October 10<sup>th</sup>.

341 By having all the precursory activity mapped and plotted into the same graph, it is  
342 easier to interpret their evolution as a whole. According to what was been defined as a  
343 significant change, in a first phase the accumulated energy released increase (AERI) and  
344 the lateral migration of seismicity (LMS) experienced a significant change, and  
345 continued overall the increasing tendency across this initial phase with periods of no  
346 significant variation followed by periods of heavy changes. By the time, they enter the  
347 second phase both indicators show no changes seem stable until well into the third  
348 phase where AERI starts experiencing significant increases and LMS follows a few  
349 days later. As per the other indicators, in a first phase they all experience a significant



350 change at some point in the initial stages of Phase I and seem to enter a quiet phase after  
351 that, except for the RSAM, which on average experiences a continuous increase across  
352 the three phases, perhaps more consistent though Phases II and III. The unrest indicators  
353 that seem to experience larger significant changes in Phase I are AERI, LMS and  
354 RSAM.

355 Phase II was characterized by an overall stabilization of the indicators, except  
356 for RSAM that continues to consistently increase. In addition, by the middle of this  
357 second phase the seismicity experiences a significant increase with a small period of  
358 significant lateral migration of seismicity, followed by a small jump in the RSAM a few  
359 days later. By the time the systems enters into the phase III on September 12 we  
360 continue to observe a probability increase in RSAM with a new significant jump around  
361 the September 18. This change happens simultaneously with a significant LMS increase  
362 for the first time since phase I, and a jump in the seismicity increase followed by an  
363 AERI jump and strain variation. There seems to be a clear inflection point around the  
364 20th of September where all unrest indicators at once, for the first time since the  
365 beginning of the unrest three months ago, begin to show consistently significant  
366 changes, indicating the system has changed and is getting ready to enter into a new  
367 eruptive phase. Note that a few days before the submarine eruption there is a jump in all  
368 the indicators including for the first time the shallow seismicity and the vertical  
369 migration of seismicity, the probabilities for these two continue to increase from this  
370 moment onwards, together with RSAM, while LMS and AERI remain constant.

371

## 372 **6. Discussion and Conclusions**

373 Short-term hazard assessment should be always conducted based on a previous long-  
374 term hazard assessment, as a systematic study of past eruptive activity conducted well



375 before a new volcanic crisis starts can help forecast the most probable scenarios and  
376 thus avoid confusion regarding the potential outcome of the forthcoming eruption.

377 In the case of El Hierro, unfortunately, no previous hazard assessment existed, so the  
378 most probable scenario – a submarine eruption – was not anticipated, as has been shown  
379 by a subsequent study (Becerril et al., 2014). Consequently, scientific advisors and  
380 decision-makers considered possible eruptive scenarios that had much lower  
381 probabilities of occurrence, which implied the taking of decisions with a higher cost  
382 than necessary (Sobradelo et al., 2014).

383 Via a retrospective analysis of the particular case of El Hierro, the results  
384 obtained in this work provide an easy and useful approach to the understanding and  
385 visualization of the information recorded by the monitoring system, and show how this  
386 information can be used to forecast an eruption and its potential hazards in real time.  
387 The translation of this information into a coherent picture that will be helpful for  
388 anticipating the future evolution of a volcanic system is not straightforward, which is  
389 why we propose that this simple methodology be used to facilitate communication  
390 among scientists and between scientists and decision-makers. Moreover, the  
391 interpretation of unrest indicators and the observation of significant variations in  
392 volcanic systems are complex tasks subject to great uncertainties and the approach  
393 proposed in this work aims to act as a guide for experts and decision-makers to be  
394 employed as a crisis unfolds.

395 Another important aspect is how to interpret monitoring signals in monogenetic  
396 volcanism. In this specific case, where the location of a future eruption is not easy to  
397 determine, the spatial probability is controlled by local and regional stress fields that are  
398 usually poorly understood. During the pre-eruptive episode on El Hierro, it was clear  
399 that the lateral migration of the magma was controlled by the presence of stress barriers



400 defined by major structural and rheological discontinuities (Martí et al. 2013, 2017).  
401 This gave rise to nearly continuous changes in the probable location of the eruptive  
402 vent, which hindered the definition of a precise eruptive scenario and the application of  
403 appropriate mitigation measures. This highlights the importance of understanding  
404 monitoring signals and their interactions, as well as the need for knowledge of the past  
405 activity of the volcanic system in the form of susceptibility and hazard analyses, if a  
406 volcanic eruption is to be correctly forecast. In case of El Hierro, the susceptibility map  
407 that combines volcano-structural information and seismic data (Fig. 3) shows how the  
408 possible location of a eruptive vent varied during the evolution of the pre-eruptive  
409 unrest: initially, the magma was thought to be accumulating on the northern side of the  
410 island (Fig. 3b) but in the end it was concentrated on the southern side (Fig. 3d), where  
411 it eventually provoked a submarine eruption. This confirms the idea that seismic activity  
412 and ground deformation are good indicators of magma location in monogenetic  
413 volcanism.

414         The analysis of the precursors shows how special attention should be paid to  
415 each one during the evolution of the unrest period (Fig. 4). Indeed, in the initial phase,  
416 we observed obvious fluctuations in most indicators and, above all, an increase in the  
417 accumulated energy released compared to the background level. In the second phase,  
418 the behavior of these indicators remained constant and there was no significant spread, a  
419 reflection of how the magma followed the local stress field and migrated from the north  
420 to the southeast. During the final month before the eruption, we noted that the indicators  
421 started to increase sequentially but at the same hypocentral depth. However, in the final  
422 hours before the eruption the presence of very shallow seismicity indicated that,  
423 immediately after the final major earthquake, a relatively rapid vertical migration of  
424 magma was taking place. This vertical ascent to the surface was associated with a



425 drastic decrease in both the number of seismic events (almost no seismicity of any kind  
426 in the 30 hours before the onset of the eruption) in the accumulated energy release, and  
427 in the deformation, but also with an increase in the RSAM, thereby suggesting that the  
428 final major tectonic earthquake facilitated a path for the magma to reach the surface  
429 (Martí et al., 2013).

430 From an emergency management perspective, it is worth stressing two further  
431 important results of the application of our method. Firstly, it identified unmistakably the  
432 anomalous behavior of the activity, characterized by an increasing probability in almost  
433 all indicators during the first days of the unrest period as they varied in relation to the  
434 background values. Secondly, many indications suggested that the probability of an  
435 eruption increased in almost all parameters from 25 September until the onset of the  
436 eruption. On 23–27 September, the Canarian Civil Protection Authorities in charge of  
437 the management of the volcanic crisis changed the alert level for the population from  
438 Green to Yellow in two areas due to the strong seismicity being felt by the population  
439 and the risk of rock falls near populated areas. In 11 October, the appearance of an  
440 increasingly strong seismic tremor signal in the monitoring network warned of the  
441 imminent onset of the eruption and Civil Protection raised the alert level to Red.  
442 Despite the correct management of the eruption crisis on El Hierro by the Canarian  
443 Civil Protection, we still believe that our results can improve significantly the island's  
444 early warning capability during an unrest period characterized by a high level of  
445 uncertainty. Thus, the tools presented here could have been very useful for the Canarian  
446 Civil Protection during the October 2011 eruption crisis.

447

448 **Acknowledgements:** This research was funded by the European Commission (EC  
449 ECHO Grant SI2.695524: VeTOOLS). The authors would like to thank the Instituto



450 Geográfico Nacional (IGN - Madrid) and, especially, Rafael Abella Meléndez, for the  
451 ease in accessing the monitoring data. Joan Martí is grateful for the MECD  
452 (PRX16/00056) grant. The English text was edited by Michael Lockwood.

453

454

455

456

457

458

459

460

461

462

463

464

465

466

467

468

469

470

471

472

473

474



475 **References**

476

477 Bartolini, S., Cappello, A., Martí, J., and Del Negro, C.: QVAST: a new Quantum GIS  
478 plugin for estimating volcanic susceptibility, *Nat. Hazards Earth Syst. Sci.*, 13, 3031–  
479 3042, doi:10.5194/nhess-13-3031-2013, 2013.

480

481 Bartolini, S., Sobradelo, R., and Martí, J.: ST-HASSET for volcanic hazard assessment:  
482 A Python tool for evaluating the evolution of unrest indicators, *Computers &  
483 Geosciences*, doi:10.1016/j.cageo.2016.05.002, 2016.

484

485 Becerril, L., Cappello, A., Galindo, I., Neri, M., and Del Negro, C.: Spatial probability  
486 distribution of future volcanic eruptions at El Hierro Island (Canary Islands, Spain), *J.  
487 Volcanol. Geoth. Res.*, 257, 21–30, doi:10.1016/j.jvolgeores.2013.03.005, 2013.

488

489 Becerril, L., Bartolini, S., Sobradelo, R., Martí, J., Morales, J.M., and Galindo, I.: Long-  
490 term volcanic hazard assessment on El Hierro (Canary Islands), *Natural Hazards and  
491 Earth System Science*, 14, 1853-1870, 2014.

492

493 Blong, R.: Volcanic hazards and risk management, in *Encyclopedia of volcanoes*, edited  
494 by H. Sigurdsson et al., pp. 1215–1227, Academic, San Diego, 2000.

495

496 Bosshard, E., and MacFarlane, D.J.: Crustal structure of the western Canary Island from  
497 seismic refraction and gravity data, *J. Geophys. Res.*, 75, 4901-4918, 1970.

498

499 Cappello, A., Neri, M., Acocella, V., Gallo, G., Vicari, A., and Del Negro, C.: Spatial  
500 vent opening probability map of Etna volcano (Sicily, Italy), *Bull. Volcanol.*, 74, 2083–  
501 2094, doi:10.1007/s00445-012-0647-4, 2012.

502

503 Carniel, R., Tárraga, M., Jaquet, O., and García, A.: On the memory of seismic noise  
504 recorded at Teide-Pico Viejo volcanic complex, Tenerife, Spain, EGU06-A-01929;  
505 NH5.03-1WE2P-0679, EGU General Assembly, Vienna, 2006.

506

507 Chouet, B.: Long period volcano seismicity: Its source and use in eruption forecasting,  
508 *Nature*, 380, 309-316. doi: 10.1038/380309a0, 1996.



- 509
- 510 Connor, C.B., and Conway, F.M.: Basaltic Volcanic Fields, in Encyclopedia of  
511 Volcanology. Academic Press, pp. 331-343, 2000.
- 512
- 513 Connor, C.B., Sparks, R.S.J., Mason, R.M., Bonadonna, C., and Young, S.R.: Exploring  
514 links between physical and probabilistic models of volcanic eruptions: The Soufrière  
515 Hills Volcano, Montserrat, *Geophys. Res. Lett.*, 30, 1701. doi:10.1029/2003GL017384,  
516 13, 2003.
- 517
- 518 Domínguez Cerdeña, I., del Fresno, C., and Gomis Moreno, A.: Seismicity patterns  
519 prior to the 2011 El Hierro eruption, *Bull. Seismol. Soc. Am.* 104, 567–575,  
520 doi:10.1785/0120130200, 2014.
- 521
- 522 Endo, T. E., and Murray, T.: Real-time Seismic Amplitude Measurement (RSAM). A  
523 volcano monitoring and prediction tool, *Bull. Volcanol.*, 53, 533–545, 1991.
- 524
- 525 Geyer, A., Martí, J., and Villaseñor, A.: First-order estimate of the Canary Islands plate-  
526 scale stress field: Implications for volcanic hazard assessment, *Tectonophysics*,  
527 doi:10.1016/j.tecto.2016.04.010, 2016.
- 528
- 529 Guillou, H., Carracedo, J.C., Pérez-Torrado, F.J., and Rodríguez Badiola, E.: K-Ar ages  
530 and magnetic stratigraphy of a hotspot- induced, fast grown oceanic island: El Hierro,  
531 Canary Islands, *J. Volcanol. Geoth. Res.* 73, 141–155, 1996.
- 532
- 533 Harrington, R.M., and Brodsky, E.E.: Volcanic hybrid earthquakes that are brittle-  
534 failure events, *Geophys. Res. Lett.*, 34, L06308, doi:10.1029/2006GL028714, 2007.
- 535
- 536 Jaquet, O., and Carniel, R.: Multivariate stochastic modelling: towards forecasts of  
537 paroxysmal phases at Stromboli, *J. Volcanol. Geotherm. Res.*, 128(1–3), 261–271,  
538 2003.
- 539
- 540 Jaquet, O., Sparks, R.S.J., and Carniel, R.: Magma memory recorded by statistics of  
541 volcanic explosions at the Soufrière Hills Volcano, Montserrat in *Statistics in*



- 542 Volcanology, Special Publications of IAVCEI, edited by Mader, H.M., S. Coles, and C.  
543 Connor, vol. 1, pp. 175–184, 2006.  
544
- 545 Jaquet, O., Connor, C.B., and Connor, L.: Probabilistic Methodology for Long Term  
546 Assessment of Volcanic Hazards, IHLRMW, Las Vegas, USA, 2008.  
547
- 548 Jellineck, A.M., and Bercovici, D.: Seismic tremors and magma wagging during  
549 explosive volcanism, *Nature*, 470, 522–526, 2011.  
550
- 551 Kereszturi, G. and Németh, K.: Monogenetic Basaltic Volcanoes: Genetic  
552 Classification, Growth, Geomorphology and Degradation, in *Updates in Volcanology-  
553 New Advances in Understanding Volcanic Systems*, edited by K. Németh, pp. 3-88,  
554 InTech, doi:10.5772/51387, 2012.  
555
- 556 Klügel, A., Hansteen, T.H., and Galipp, K.: Magma storage and underplating beneath  
557 Cumbre Vieja volcano, La Palma (Canary Islands), *Earth and Planetary Science Letters*  
558 236, 211–226, 2005.  
559
- 560 Lavallée, Y., Meredith, P.G., Dingwell, D.B., Hess, K.U., Wassermann, J., Cordonnier,  
561 B., Gerik, A., and Kruhl, J.H.: Seismogenic lavas and explosive eruption forecasting,  
562 *Nature*, 453, 507–510, 2008.  
563
- 564 López, C., Blanco, M.J., Abella, R., Brenes, B., Cabrera-Rodríguez, V.M., Casas, B.,  
565 Domínguez-Cerdeña, I., Felpeto, A., Fernández de Villalta, M., del Fresno, C., García,  
566 O., García-Arias, M.J., García-Cañada, L., Gomis-Moreno, A., González-Alonso, E.,  
567 Guzmán-Pérez, J., Iribarren, I., López-Díaz, R., Luengo-Oroz, N., Meletlidis, S.,  
568 Moreno, M., Moure, D., Pereda de Pablo, J., Rodero, C., Romero, E., Sainz-Maza, S.,  
569 Sentre-Domingo, M.A., Torres, P.A., Trigo, P., and Villasante-Marcos, M.: Monitoring  
570 the unrest of El Hierro (Canary Islands) before the onset of the 2011 Submarine  
571 Eruption, *Geophys. Res. Lett.*, 39, L13303, doi:10.1029/2012GL051846, 2012.  
572
- 573 López, C., Martí, J., Abella, R., and Tárrega, M.: Applying fractal dimensions and  
574 energy-budget analysis to characterize fracturing processes during magma migration



- 575 and eruption: 2011–2012 El Hierro (Canary Islands) submarine eruption, *Surv.*  
576 *Geophys.* 1–22, doi:10.1007/s10712-014-9290-2, 2014.
- 577
- 578 López, C., Benito-Saz, M. A., Martí, J., del-Fresno, C., García-Cañada, L., Albert, H.,  
579 Lamolda, H.: Driving Magma to the Surface: the 2011–2012 El Hierro Volcanic  
580 Eruption. *Geochemistry, Geophysics, Geosystems* (submitted).
- 581 Martí, J., Pinel, V., López, C., Geyer, A., Abella, R., Tárraga, M., Blanco, M.J., Castro,  
582 A., and Rodríguez, C.: Causes and mechanisms of the 2011–2012 El Hierro (Canary  
583 Islands) submarine eruption, *J. Geophys. Res. B: Solid Earth*, 118(3), 823–839.  
584 doi:<http://dx.doi.org/10.1002/jgrb.50087>, 2013.
- 585
- 586 Martí, J., López, C., Bartolini, S., Becerril, L., and Geyer, A.: Stress controls of  
587 monogenetic volcanism: a review, *Frontiers in Earth Sciences*, 4(106). doi:  
588 10.3389/feart.2016.0010, 2016.
- 589
- 590 Martí, J., A. Villaseñor, A. Geyer, C. López, and Tryggvason, A.: Stress barriers  
591 controlling lateral migration of magma revealed by seismic tomography, *Scientific*  
592 *Reports*, 7, 40757, doi: 10.1038/srep40757, 2017.
- 593
- 594 Martin, A.J., Umeda, K., Connor, C.B., Weller, J.N., Zhao, D., and Takahashi, M.:  
595 Modeling long-term volcanic hazards through Bayesian inference: an example from the  
596 Tohoku volcanic arc Japan, *J. Geophys. Res.*, 109, B10208,  
597 doi:10.1029/2004JB003201, 2004.
- 598
- 599 Marzocchi, W., Sandri, L., and Selva, J.: BET\_EF: A probabilistic tool for long- and  
600 short-term eruption forecasting, *Bull. Volcanol.*, 70, 623–632, 2008.
- 601
- 602 McNutt, S.: Seismic monitoring and eruption forecasting of volcanoes: A review of the  
603 state of the art and case histories, in *Monitoring and mitigation of volcano hazards*,  
604 edited by Scarpa and Tilling, Springer, Berlin, 99–146, 1996.
- 605
- 606 McNutt, S. R.: Volcano Seismology, *Ann. Rev. Earth Planet. Sci.*, 33, 461–491, 2005.
- 607



- 608 Neuberg, J., Luckett, R., Baptie, B., and Olsen, K.: Models of tremor and low-frequency  
609 earthquake swarms on Montserrat, *J. Volcanol. Geoth. Res.*, 101, 83–104, 2000.  
610
- 611 Papale, P.: Strain-induced magma fragmentation in explosive eruptions, *Nature* 397,  
612 425–428, 1999.  
613
- 614 Phillipson, G., Sobradelo, R., and Gottsmann, J.: Global volcanic unrest in the 21st  
615 century: An analysis of the first decade, *J. Volcanol. Geoth. Res.*, 264, 183–196, 2013.  
616
- 617 Ranero, C.R., Torne, M., and Banda, E.: Gravity and multichannel seismic reflection  
618 constraints on the lithospheric structure of the Canary swell, *Mar. Geophys. Res.*, 17,  
619 519–534, 1995.  
620
- 621 Scarpa, R., and Tilling, R.I.: *Monitoring and Mitigation of Volcano Hazards*: Berlin,  
622 Springer-Verlag, 1996.  
623
- 624 Silverman, B.W.: *Density Estimation for Statistics and Data Analysis*, Chapman & Hall,  
625 London, 1986.  
626
- 627 Sparks, R.S.J.: Forecasting volcanic eruptions, *Earth Planet. Sci. Lett.*, 210, 1–15, 2003.  
628
- 629 Sobradelo, R., Martí, J., Kilburn, C., and López, C.: Probabilistic approach to decision-  
630 making under uncertainty during volcanic crises: retrospective application to the El  
631 Hierro (Spain) 2011 volcanic crisis, *Nat. Hazards*, doi:10.1007/s11069-014-1530-8,  
632 2014.  
633
- 634 Sobradelo, R., and Martí, J.: Short-term volcanic hazard assessment through Bayesian  
635 inference: Retrospective application to the Pinatubo 1991 volcanic crisis, *Journal of*  
636 *Volcanology and Geothermal Research*, 290, 1–11, 2015.  
637
- 638 Stein, R.: The role of stress transfer in earthquake occurrence, *Nature* 402, 605–609,  
639 1999.  
640



- 641 Stroncik, N. A, Klügel, A., and Hansteen, T.H.: The magmatic plumbing system  
642 beneath El Hierro (Canary Islands): constraints from phenocrysts and naturally  
643 quenched basaltic glasses in submarine rocks. *Contrib. Mineral. Petrol.*, 157, 593-607,  
644 doi:10.1007/s00410-008-0354-5, 2009.
- 645
- 646 Tárrega, M., Carniel, R., Ortiz, R., Marrero, J.M., and García, A.: On the predictability  
647 of volcano- tectonic events by low frequency seismic noise analysis at Teide-Pico Viejo  
648 volcanic complex, Canary Islands, *Natural Hazards and Earth System Science*, 6(3),  
649 365-376, 2006.
- 650
- 651 Tárrega, M., Martí, J., Abella, R., Carniel, R., and López, C.: Volcanic tremors: good  
652 indicators of change in plumbing systems during volcanic eruptions, *J. Volcanol.*  
653 *Geotherm. Res.*, 273, doi:j.jvolgeores.01.003, 2014.
- 654
- 655 Telesca, L., Lovallo, M., Martí, J., López, C., and Abella, R.: Using the Fisher–Shannon  
656 method to characterize continuous seismic signal during volcanic eruptions: application  
657 to 2011–2012 El Hierro (Canary Islands) eruption. Revealing dynamic changes on El  
658 Hierro (Canary Islands) during the 2011–2012 eruption through investigation of the  
659 continuous seismic signal. *Terra Nova*, 26, 425–429, 2014.
- 660
- 661 Telesca, L., Lovallo, M., Martí, J., López, C., and Abella, R.: Multifractal investigation  
662 of continuous seismic signal recorded at El Hierro volcano (Canary Islands) during the  
663 2011–2012 pre- and eruptive phases, *Tectonophysics*, 642, 71–77, 2015.
- 664
- 665 Tonini, R., Sandri, L., Rouwet, D., Caudron, C., Marzocchi, W., and Suparjan: A new  
666 Bayesian Event Tree tool to track and quantify volcanic unrest and its application to  
667 Kawah Ijen volcano, *Geochem. Geophys. Geosyst.*, 17, 2539–2555,  
668 doi:10.1002/2016GC006327, 2016.
- 669
- 670 Valentine, G.A., and Gregg, T.K.P.: Continental basaltic volcanoes-processes and  
671 problems, *J. Volcanol. Geotherm. Res.*, 177(4), 857–873, 2008.
- 672



673 Vallianatos, F., Michas, G., Papadakis, G., and Tzani, A.: Evidence of non-extensivity  
674 in the seismicity observed during the 2011–2012 unrest at the Santorini volcanic  
675 complex, Greece, Nat. Hazards Earth Syst. Sci., 13, 177–185, 2013.

676

677 Watts, A.B.: Crustal structure, gravity-anomalies and flexure of the lithosphere in the  
678 vicinity of the Canary-Islands. Geophys. J. Int. 119 (2), 648-666, doi:10.1111/j.1365-  
679 246X.1994.tb00147.x, 1994.

680

681

682

683

684

685

686

687

688

689

690

691

692

693

694

695

696

697

698

699



700 **Table**

701 Table 1. Unrest indicators during the unrest period.

702

703 **Figures**

704 Figure 1. Location of El Hierro and the IGN monitoring network during the unrest  
705 period.

706 Figure 2. Structural data of El Hierro and the evolution of the seismicity during the  
707 unrest period (average location of the seismic swarm).

708 Figure 3. Susceptibility maps obtained from: a) the volcano-structural data; b) the first  
709 days of unrest; c) in the middle of the unrest; d) the days before the submarine eruption.

710 Figure 4. ST-HASSET: the evolution of the unrest indicators in three phases of 28 days.  
711 The right side of the chart shows day-by-day the tendency of variation of the unrest  
712 indicators.

713 Figure 5. ST HASSET: the evolution of all indicators every 28 days (3 phases of  
714 unrest).

715

716 **Supplementary Material**

717 Figure S1 - Susceptibility maps and seismicity location during the evolution of the  
718 unrest period.

719 Movie S1 - Evolution of the unrest indicators and its registered values.



Table 1

UNREST INDICATORS	SEISMICITY INCREASE			RSAM ACCELERATION INCREASE			ACCUMULATED ENERGY RELEASED INCREASE			LATERAL MIGRATION OF SEISMICITY			VERTICAL MIGRATION OF SEISMICITY			SHALLOW SEISMICITY			STRAIN VARIATION		
	YN/na	Value [m <sup>2</sup> ]	Probability	YN/na	Value [RSAM unit]	Probability	YN/na	Value [J]	Probability	YN/na	(Figure 2)	Probability	YN/na	Value [m]	Probability	YN/na	Value [m <sup>2</sup> ]	Probability	YN/na	Value [m]	Probability
2011-07-19	N	0	0.303	N	24.62	0.303	N	5.90E+07	0.303	N	0.303	N	12	0.303	N	0	0.303	N	0.102	0.303	
2011-07-20	N	0	0.25	N	20.80	0.250	Y	2.41E+08	0.500	Y	0.500	N	11.88	0.250	N	0	0.25	N	0.014	0.25	
2011-07-21	N	0	0.2	N	25.38	0.200	Y	1.72E+09	0.600	N	0.400	N	10.78	0.200	N	0	0.2	N	0.015	0.2	
2011-07-22	N	0	0.167	N	23.34	0.167	Y	3.18E+09	0.667	N	0.333	N	10.09	0.167	N	0	0.167	N	0.015	0.167	
2011-07-23	N	0	0.143	N	21.21	0.143	Y	2.15E+09	0.715	Y	0.428	N	10.72	0.143	N	0	0.143	N	0.014	0.143	
2011-07-24	N	0	0.125	N	19.55	0.125	Y	4.30E+09	0.751	Y	0.499	N	10.53	0.125	N	0	0.125	N	0.012	0.125	
2011-07-25	N	0	0.111	N	18.66	0.111	Y	5.73E+09	0.779	Y	0.555	Y	13.4	0.222	N	0	0.111	N	0.014	0.111	
2011-07-26	N	0	0.1	N	19.02	0.100	Y	1.50E+09	0.801	N	0.499	N	8.45	0.200	N	1	0.1	N	0.014	0.1	
2011-07-27	Y	2	0.182	N	19.19	0.091	Y	3.00E+09	0.819	N	0.454	N	8.93	0.182	Y	4	0.182	N	0.015	0.091	
2011-07-28	N	0	0.167	Y	18.26	0.167	Y	7.27E+08	0.834	N	0.416	N	10.33	0.167	N	1	0.167	N	0.016	0.083	
2011-07-29	N	0	0.154	Y	22.92	0.231	N	1.79E+08	0.770	N	0.384	N	12.75	0.154	N	0	0.154	N	0.016	0.077	
2011-07-30	N	0	0.143	Y	27.70	0.286	N	6.17E+08	0.715	N	0.357	Y	11.82	0.214	N	0	0.143	N	0.018	0.071	
2011-07-31	N	0	0.133	N	28.73	0.267	N	1.22E+09	0.667	N	0.333	N	11.18	0.200	N	0	0.133	na	na	0.071	
2011-08-01	N	0	0.125	N	25.78	0.250	N	1.75E+08	0.625	N	0.312	N	12	0.188	N	0	0.125	N	0.020	0.067	
2011-08-02	N	0	0.118	N	21.44	0.235	N	4.60E+08	0.588	Y	0.352	N	10.67	0.177	N	0	0.118	N	0.017	0.063	
2011-08-03	N	0	0.111	N	22.17	0.222	N	4.48E+08	0.555	Y	0.388	N	11.47	0.167	N	0	0.111	N	0.020	0.059	
2011-08-04	N	0	0.105	N	23.72	0.210	Y	2.80E+09	0.578	Y	0.420	N	10.54	0.158	N	0	0.105	N	0.021	0.056	
2011-08-05	N	0	0.1	N	26.11	0.199	Y	4.24E+09	0.599	Y	0.449	N	10.54	0.150	N	1	0.1	N	0.020	0.053	
2011-08-06	N	0	0.095	N	24.29	0.190	Y	2.31E+08	0.618	Y	0.475	N	9.61	0.143	N	0	0.095	N	0.022	0.05	
2011-08-07	N	0	0.091	N	17.88	0.181	Y	1.62E+09	0.635	N	0.453	N	10.45	0.136	N	3	0.091	Y	0.027	0.063	
2011-08-08	N	0	0.087	Y	15.15	0.217	N	1.46E+09	0.607	N	0.433	N	11.16	0.130	N	1	0.087	N	0.022	0.069	
2011-08-09	Y	1	0.125	Y	18.75	0.250	Y	4.38E+09	0.623	N	0.415	N	10.6	0.125	N	2	0.083	N	0.021	0.065	
2011-08-10	N	0	0.12	Y	26.84	0.280	Y	1.58E+09	0.638	N	0.398	N	10.95	0.120	N	0	0.08	N	0.024	0.062	
2011-08-11	N	0	0.115	N	28.53	0.269	N	4.12E+08	0.613	N	0.383	N	10.07	0.115	N	0	0.077	N	0.023	0.079	
2011-08-12	N	0	0.111	N	26.71	0.259	N	2.72E+08	0.590	N	0.369	N	11.28	0.111	N	0	0.074	N	0.022	0.076	
2011-08-13	N	0	0.107	N	27.61	0.250	N	6.22E+07	0.569	Y	0.392	N	10	0.107	N	0	0.071	N	0.021	0.073	
2011-08-14	N	0	0.103	N	28.80	0.241	N	1.40E+09	0.549	Y	0.413	N	11.91	0.103	N	0	0.069	N	0.021	0.07	
2011-08-15	N	0	0.1	N	26.39	0.233	N	6.61E+08	0.531	N	0.396	N	11.41	0.100	N	0	0.067	N	0.024	0.068	
2011-08-16	N	0	0.097	N	24.65	0.225	N	1.72E+08	0.514	Y	0.418	N	11.47	0.097	N	0	0.065	N	0.023	0.066	
2011-08-17	N	0	0.094	N	28.33	0.218	N	6.46E+07	0.498	Y	0.436	N	10.9	0.094	N	0	0.063	N	0.023	0.064	
2011-08-18	N	0	0.091	N	22.92	0.211	N	4.55E+09	0.483	Y	0.453	N	10.59	0.091	N	2	0.061	N	0.023	0.062	
2011-08-19	N	0	0.088	N	17.42	0.205	Y	2.16E+09	0.498	Y	0.449	N	10.52	0.088	N	2	0.059	N	0.023	0.06	
2011-08-20	N	0	0.085	Y	15.38	0.228	N	1.75E+08	0.484	N	0.458	N	11.15	0.085	N	0	0.057	N	0.024	0.058	
2011-08-21	N	0	0.083	Y	18.33	0.246	N	2.25E+09	0.471	N	0.443	N	11.12	0.083	N	0	0.055	N	0.025	0.056	
2011-08-22	N	0	0.081	Y	22.89	0.269	N	2.72E+09	0.458	Y	0.458	N	11.12	0.081	Y	4	0.081	N	0.026	0.054	
2011-08-23	N	0	0.079	Y	25.08	0.286	N	1.11E+09	0.446	Y	0.472	N	10.97	0.079	N	0	0.079	N	0.026	0.053	
2011-08-24	N	0	0.077	N	24.26	0.281	N	3.55E+07	0.435	N	0.460	N	10.32	0.077	N	0	0.077	N	0.024	0.052	
2011-08-25	N	0	0.075	N	19.57	0.274	N	2.55E+08	0.424	N	0.449	N	10.75	0.075	N	0	0.075	N	0.025	0.051	
2011-08-26	N	0	0.073	N	17.38	0.267	N	5.78E+07	0.414	Y	0.462	N	10.9	0.073	N	0	0.073	N	0.026	0.05	
2011-08-27	N	0	0.071	Y	16.03	0.284	N	1.17E+09	0.404	N	0.451	N	11.23	0.071	N	0	0.071	N	0.025	0.049	
2011-08-28	N	0	0.069	Y	17.48	0.301	N	2.56E+07	0.395	N	0.441	N	10.95	0.069	N	0	0.069	N	0.028	0.048	
2011-08-29	N	0	0.067	Y	24.46	0.317	N	2.42E+08	0.386	N	0.431	N	10.69	0.067	N	0	0.067	N	0.027	0.047	
2011-08-30	N	0	0.066	N	20.40	0.310	N	6.00E+08	0.377	N	0.421	N	10.71	0.066	N	0	0.066	N	0.028	0.046	
2011-08-31	N	0	0.065	N	11.87	0.303	N	7.45E+08	0.369	N	0.412	N	11.61	0.065	N	1	0.065	N	0.027	0.045	
2011-09-01	Y	1	0.085	Y	8.20	0.318	N	4.35E+09	0.361	N	0.403	N	11.2	0.064	N	0	0.064	N	0.028	0.044	
2011-09-02	Y	2	0.104	Y	11.11	0.332	N	3.96E+09	0.353	N	0.395	N	11.02	0.063	N	1	0.063	N	0.031	0.043	
2011-09-03	N	0	0.102	Y	16.66	0.346	N	1.28E+09	0.346	N	0.387	N	11.14	0.062	N	1	0.062	N	0.030	0.042	
2011-09-04	N	0	0.1	Y	18.58	0.359	N	8.43E+08	0.339	Y	0.399	N	10.79	0.061	N	0	0.061	N	0.030	0.041	
2011-09-05	N	0	0.098	N	18.58	0.352	N	5.58E+08	0.332	Y	0.411	N	10.69	0.060	N	0	0.06	N	0.030	0.04	
2011-09-06	N	0	0.096	N	20.50	0.345	N	7.45E+08	0.326	N	0.403	N	10.38	0.059	N	2	0.059	N	0.031	0.039	
2011-09-07	N	0	0.094	N	18.18	0.338	N	1.40E+09	0.320	N	0.395	N	10.93	0.058	N	1	0.058	N	0.030	0.038	
2011-09-08	N	0	0.092	Y	15.87	0.350	N	9.15E+08	0.314	N	0.388	N	10.94	0.057	N	1	0.057	N	0.030	0.037	
2011-09-09	N	0	0.09	Y	17.73	0.382	N	1.60E+09	0.308	N	0.381	N	11.4	0.056	N	0	0.056	N	0.029	0.036	
2011-09-10	Y	1	0.106	Y	21.18	0.373	N	1.88E+09	0.303	N	0.374	N	11.27	0.055	N	0	0.055	N	0.034	0.035	
2011-09-11	N	0	0.104	N	19.77	0.366	N	6.27E+08	0.298	N	0.367	N	11.25	0.054	N	0	0.054	N	0.032	0.034	
2011-09-12	Y	3	0.119	N	19.89	0.360	N	3.87E+09	0.293	N	0.361	N	11.19	0.053	N	0	0.053	N	0.034	0.033	
2011-09-13	N	1	0.117	N	22.36	0.354	N	2.34E+09	0.288	N	0.355	N	11.55	0.052	N	0	0.052	N	0.033	0.032	
2011-09-14	N	0	0.115	N	20.04	0.348	N	7.86E+08	0.283	N	0.349	N	11.4	0.051	N	0	0.051	N	0.038	0.031	
2011-09-15	N	0	0.113	N	17.08	0.342	N	9.42E+08	0.278	Y	0.350	N	11.63	0.050	N	0	0.05	N	0.034	0.03	
2011-09-16	N	0	0.111	Y	16.50	0.353	N	4.77E+08	0.274	N	0.354	N	12.07	0.049	N	0	0.049	N	0.036	0.03	
2011-09-17	N	0	0.109	Y	19.98	0.363	N	5.50E+08	0.270	N	0.348	N	12.59	0.048	N	0	0.048	N	0.038	0.03	
2011-09-18	N	0	0.107	Y	24.37	0.373	N	1.09E+09	0.266	N	0.343	N	12.76	0.047	N	0	0.047	N	0.038	0.03	
2011-09-19	N	0	0.105	Y	25.80	0.383	N	5.71E+08	0.262	N	0.338	N	12.51	0.046	N	0	0.046	Y	0.042	0.046	
2011-09-20	Y	8	0.119	Y	28.77	0.392	N	8.51E+09	0.258	N	0.333	N	12.57	0.045	N	0	0.045	N	0.041	0.044	
2011-09-21	N	2	0.117	N	26.78	0.386	N	1.69E+09	0.254	N	0.328	N	12.52	0.044	N	1					



Figure 1

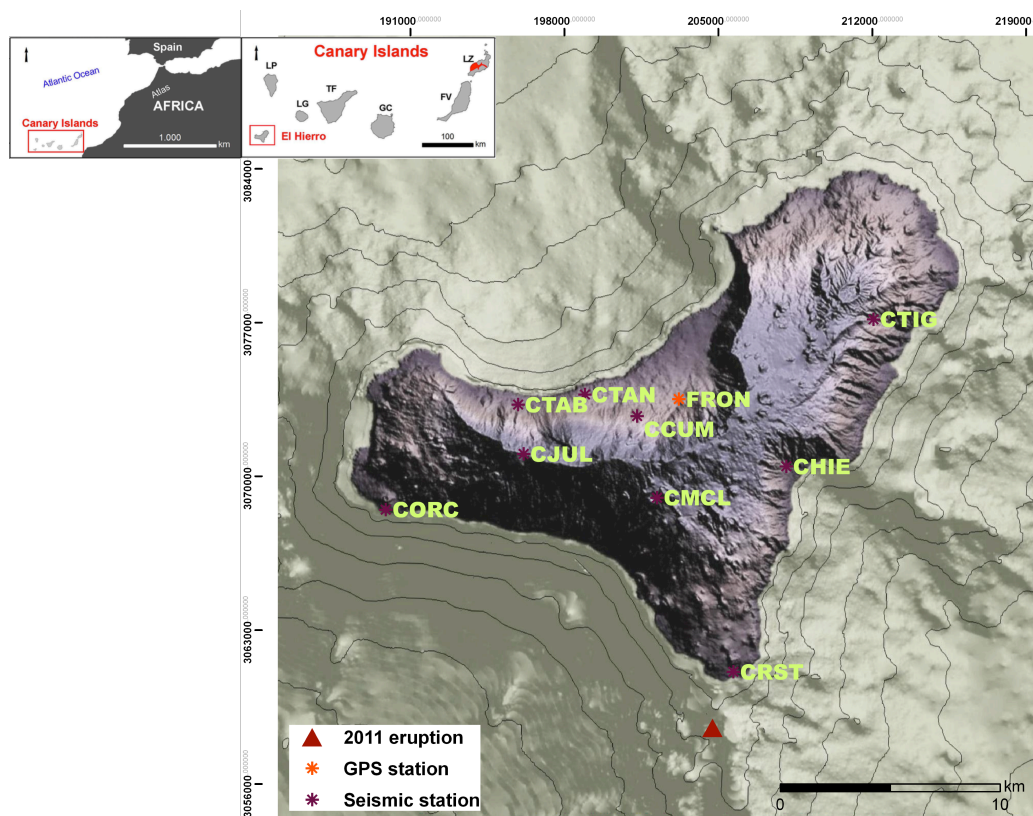




Figure 2

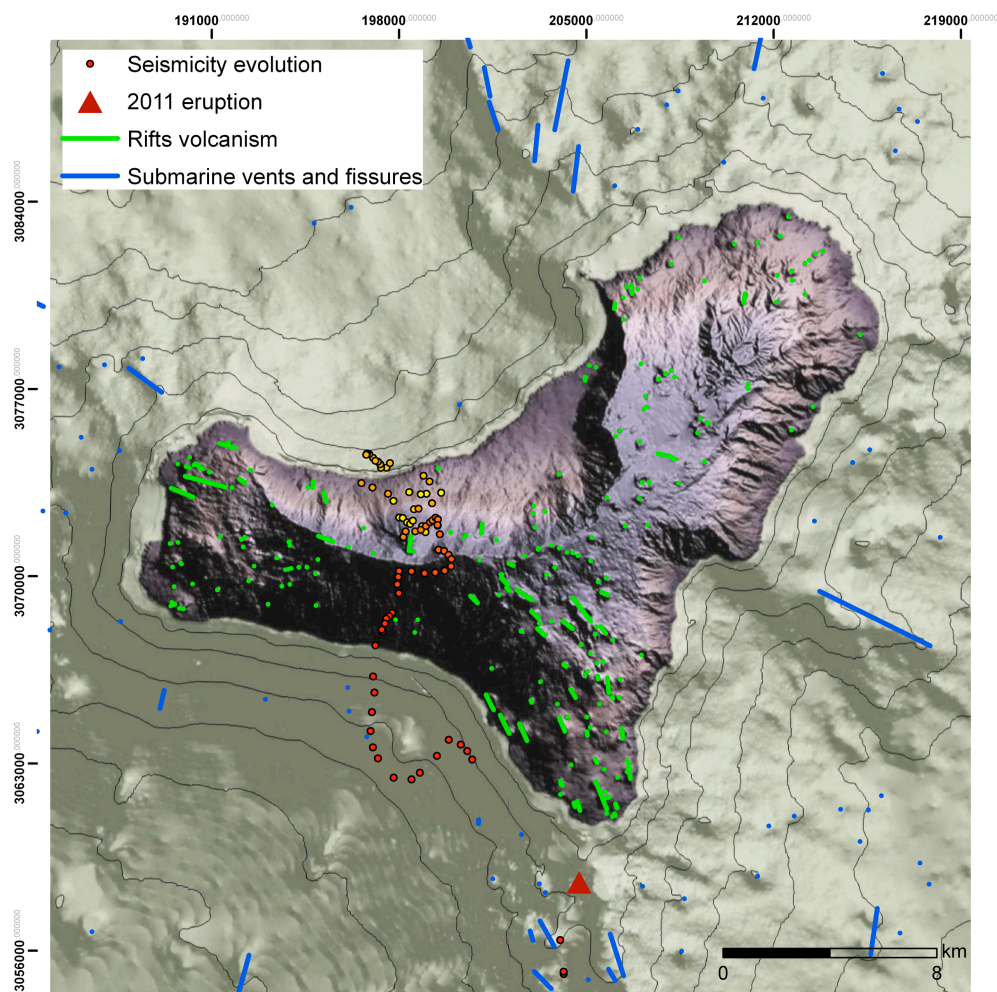




Figure 3

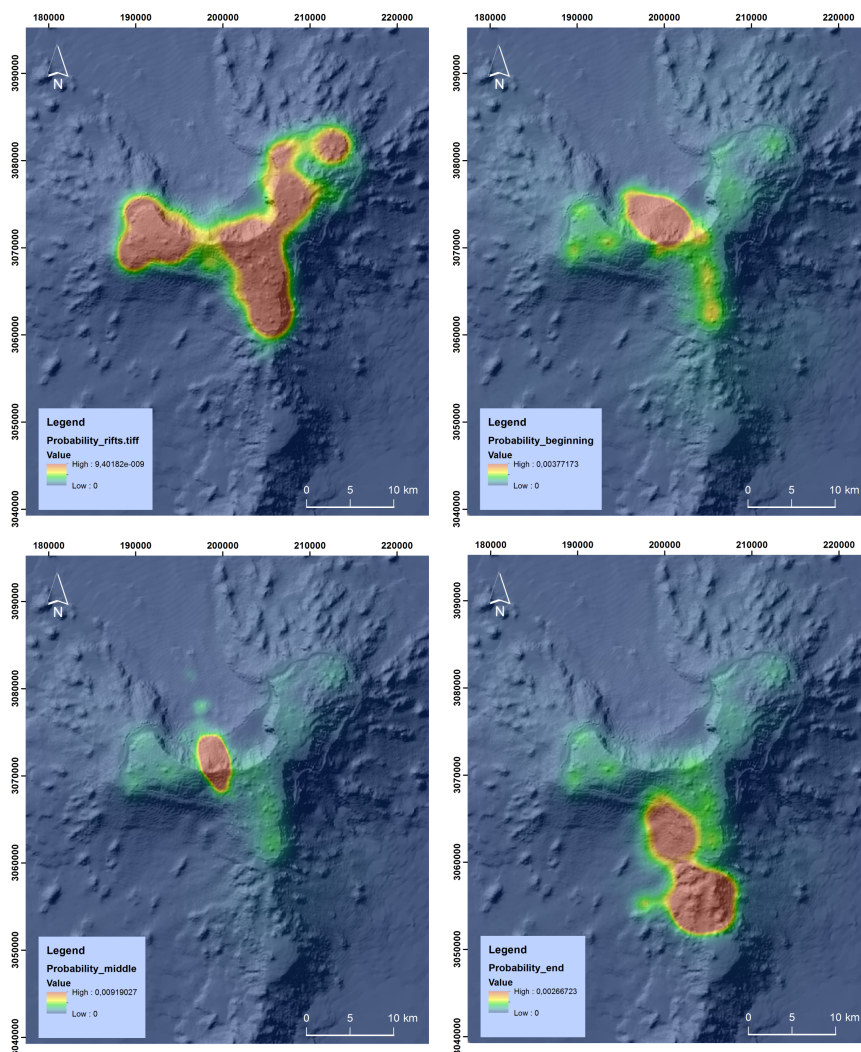




Figure 4

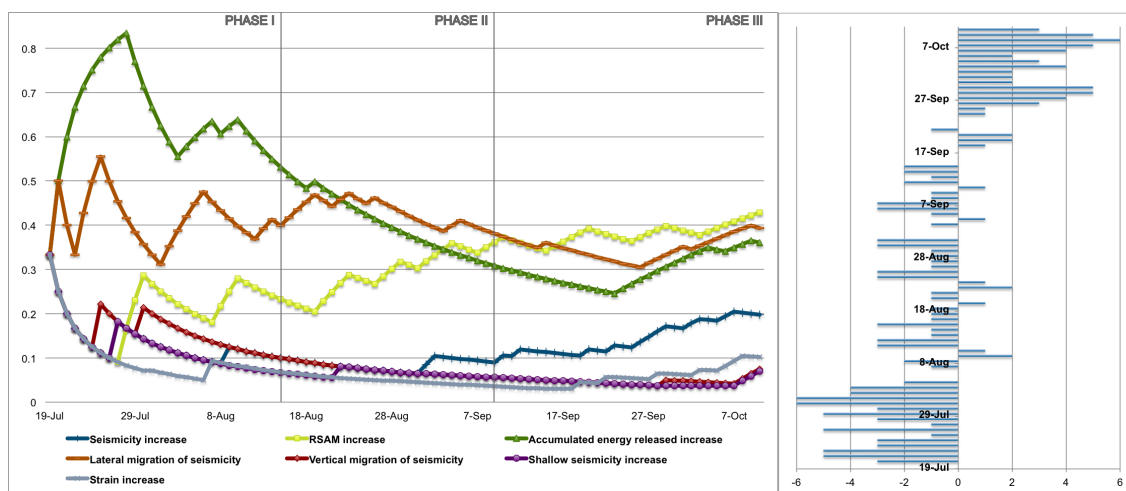




Figure 5

